Available online at www.sciencedirect.com

ScienceDirect

Advances in Space Research 73 (2024) 4414–4425

ADVANCES IN SPACE RESEARCH (a COSPAR publication)

www.elsevier.com/locate/asr

Synchronous observations of traveling ionospheric disturbances by the multipoint Doppler sounding, ionosonde and the incoherent scatter radar: Case study

Kateryna D. Aksonova [a,b,*], Andrii O. Sopin [c,d], Dalia Burešová [b], Andriy V. Zalizovski [c,d,e], Ihor F. Domnin [a]

[a] Institute of Ionosphere, 16 Kyrpychova Str., Kharkiv 61002, Ukraine
[b] Institute of Atmospheric Physics of the Czech Academy of Science, Bocni II 1401/1A, Prague 14100, Czech Republic
[c] Institute of Radio Astronomy of the National Academy of Sciences of Ukraine, 4 Mystetstv Str., Kharkiv 61002, Ukraine
[d] State Institution National Antarctic Scientific Center of the Ministry of Education and Science of Ukraine, 16 Taras Shevchenko Blvd., Kyiv 01601, Ukraine
[e] Space Research Centre of Polish Academy of Sciences, 18a Bartycka Str., Warszawa 00-716, Poland

Received 1 November 2023; received in revised form 9 January 2024; accepted 17 January 2024
Available online 19 January 2024

Abstract

In this paper, we present the results of a special experimental study of quiet-time behavior of the mid-latitude ionosphere over Eastern Europe by synchronously operation of different ground-based facilities. For the first time we used data obtained from Kharkiv incoherent scatter (IS) radar, ionosonde and coherent Doppler HF sounding system to detect and investigate traveling ionospheric disturbances (TIDs). The periods close to winter solstice and autumn equinox in 2018 were analyzed. The dominant periods and horizontal phase velocities of registered TIDs were 45–80 min and 230–460 m s^{-1}, respectively. The strongest signatures were observed in the solstice measurement and represented by large amplitudes. Based on results obtained by all three methods, we found the LS TIDs with the same interval of time and altitude of propagation and similar characteristics (the period of about 50 min, estimated vertical 80 m/s and horizontal 460 m/s velocity and horizontal spatial scale size about 1360 km) for winter measurement. Such observational findings confirm the reliability of these TID detection techniques. Possible sources of TIDs generation were considered including solar terminator.

Keywords: Incoherent scatter radar; Doppler sounding; Mid-latitude ionosphere; Traveling ionospheric disturbances; Quiet geomagnetic conditions; Solar terminator

1. Introduction

The wave mechanism is one of the effective mechanisms of coupling between the layers of the atmosphere. It is generally accepted to highlight a group of oscillations that may propagate over considerable distances without changing its form. These oscillations are commonly referred to as traveling ionospheric disturbances (TIDs). Daytime TIDs are the manifestations of acoustic-gravity waves (AGWs) (Hines, 1960; Fritts et al., 2018; Nishimura et al., 2020; Zawdie et al., 2022), while nighttime TIDs may be a non-AGWs related (Medvedev et al., 2017). For several decades, such wave heterogeneities were studied both experimentally and theoretically (Hocke and Schlegel, 1996; Belehaki et al., 2020; Tsagouri et al., 2023). TIDs at mid-latitudes have been observed in several longitudinal sectors and with different observational techniques, such as

* Corresponding author.
E-mail addresses: katya.aksen93@gmail.com (K.D. Aksonova), sopin@rian.kharkov.ua (A.O. Sopin), buresd@ufa.cas.cz (D. Burešová), zaliz@rian.kharkov.ua (A.V. Zalizovski).

https://doi.org/10.1016/j.asr.2024.01.032
0273-1177/

high-frequency (HF) Doppler sounders, ionosondes, incoherent scatter (IS) radars, optical techniques and GPS-networks, etc. (Waldock and Jones, 1986; Shiokawa, et al., 2003; Bowman, 1990; Ogawa et al., 2009). The TIDs tracking is very important because they affect all services that rely on predictable ionospheric conditions for radio wave propagation. TIDs are often divided into three classes: small-scale (SS), medium-scale (MS) and large-scale (LS) TIDs. SS disturbances have periods T of several minutes, horizontal wavelengths Λ_h of 10–100 km and horizontal phase velocities V_h of several dozen meters per second. MS TIDs has typical Λ_h of several hundred kilometers, V_h of 100–250 m/s, and T of 15–60 min, whereas LSTIDs characterized by Λ_h of more than 1000 km, $V_h = (400–1000)$ m/s and $T = (60–180)$ min (Hocke and Schlegel, 1996).

Interest in these types of disturbances has grown because their sources could be different and mechanisms of generation are still not completely explained. One of the regular sources of quiet-time TIDs is the solar terminator (ST) (Somsikov, 2011). This is due to sharp changes in atmospheric parameters such as temperature, pressure and electron concentration at a given height. Auroral processes and geomagnetic storms are the most important sources which generate wave packets and can lead to significant regional or even global changes in the ionosphere (Hunsucker, 1982; Lyons et al., 2019; Lyons et al., 2021), as well as variety of strong irregular meteorological events, tsunamis, typhoons, tropical cyclones, earthquakes, solar eclipses (Suzuki et al., 2013; Azeem et al., 2015; Nenovski et al., 2010; Vadas et al., 2015). Some authors state that MSTIDs may be observed during all days, seasons, and geomagnetic conditions, whereas LSTIDs are related to geomagnetic storms and substorms. Our previous study (Aksonova and Panasenko, 2020) refuted such conclusions. The LSTIDs were found to occur in both the magnetically quiet and disturbed days. Despite the progress made in the reconstruction of the ionospheric wave structures, determination and prediction of their parameters remains a challenging problem.

In this paper, we analyze measurements from multipoint HF Doppler ionospheric sounding facility, Kharkiv incoherent scatter (IS) radar and an ionosonde to observe TIDs during characteristic geophysical periods (experiments were carried out near the autumnal equinox and winter solstice 2018). This is the first-time report of such synchronous measurements of TID parameters over Ukraine region.

The simultaneous use of several methods of remote sounding of the ionosphere expands the possibilities for studying the characteristics of AGWs/TIDs. Determination of space–time structures that extend at ionospheric heights, elucidation of their causes and time of occurrence, perturbation strength, the speed and direction of propagation, according to the data of only one radio-physical instrument, is often difficult or impossible. Joint analysis of data from several tools significantly improves the situation. The paper aims to illustrate the possibilities of combined diagnostics of TIDs over the Ukraine using the IS radar, ionosonde, and coherent Doppler HF sounding system.

2. Scheme of experiment

2.1. Kharkiv incoherent scatter radar

One of the facilities involved in this work is the Kharkiv IS radar. The IS technique is one of the most efficient ground-based radio-physical methods to investigate the ionosphere and to study TID characteristics. Kharkiv IS radar is located at the observatory of the Institute of Ionosphere (Domnin et al., 2014). The geographic coordinates are 49.6°N, 36.3°E. It is the only instrument that uses the method of incoherent scattering to study the state of the ionosphere over mid-latitude Europe. The radar operates with 100-m zenith pointing parabolic antenna and signals with circular polarization to avoid Faraday fading IS echoes. The operating frequency is about 158 MHz. The measurements were carried out by two radio pulses of long (663 μs) and short (135 μs) durations. The height resolution is 20 km for variations in the received signal power δP and approximately 100 km for plasma temperatures. The investigated altitude range is from 100 to 1500 km.

2.2. Multipoint facility for HF Doppler sounding of the ionosphere

A multipoint HF Doppler measuring system was developed in the Institute of Radio Astronomy of the National Academy of Sciences of Ukraine (IRA NASU) for remote sensing of the ionospheric disturbances (Zalizovski et al., 2021). The system was launched in Kharkiv region at IRA NASU observatories in early 2018. Fig. 1 shows positions of the transmitter (KHR, 50.05°N, 36.29°E) and three receiving sites: Low Frequency Observatory (LFO, 49.93° N, 36.96°E), S. Braude Radio Astronomical Observatory (RAO, 49.64°N, 36.94°E), and South-West Kharkiv (SWK, 49.95°E, 36.14°N) where the data were collected.

The HF sounding system operates continuously at fixed sounding frequency (approximately 3.7 MHz) measuring amplitude and Doppler frequency shift of ionospherically reflected HF signal. The transmitted power radiated using 30-meter symmetric horizontal antenna is less than 100 W in continuous wave mode of operation. All receiving sites are similar and equipped with the identical HF Doppler system, developed in IRA NASU (Koloskov et al., 2014), and are made based on software-defined radio technology using digital WiNRADiO receiver WR-G313i. All three stations receive signals using 10-meter symmetrical horizontal antennas. The output signal is registered in ~500 Hz bandwidth. Receiving stations are equipped with Internet-based systems for remote control, data collection, processing, and visualization in the form of dynamic spectra.

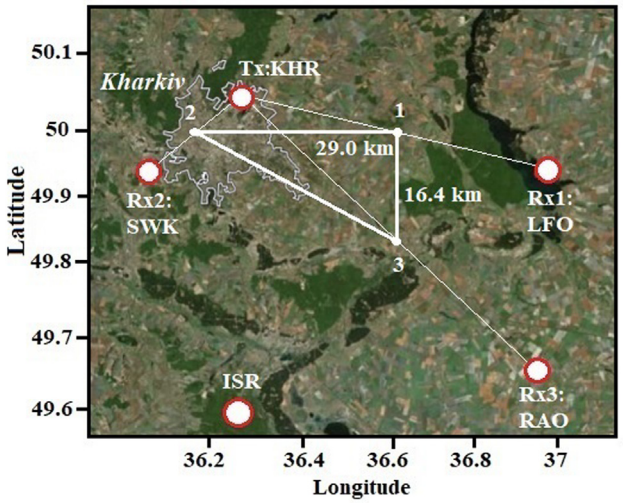

Fig. 1. Scheme of HF Doppler measurements. The location of the Kharkiv IS radar and ionosonde is marked as ûISRý. The position of the transmitting (Tx) and receiving (Rx1–Rx3) sites of the HF Doppler sounding facility, as well as the projection of the midpoints of ionospheric paths or reflection points of the HF signal from the ionosphere (listed on the map by the numbers 1–3), and the horizontal distances between them are indicated.

2.3. Doppler ionosonde

Measurements of ionospheric parameters were provided by portable Doppler ionosonde (Zalizovski et al., 2018; Koloskov et al., 2023) which allows to measure in addition to standard ionograms the Doppler frequency shifts (DFS) of reflected signals on different carrier frequencies and estimate the line-of-sight projection of plasma velocity in a wide range of heights. The system of Doppler vertical sounding of the ionosphere is installed at the territory of the observatory of the Institute of Ionosphere, where Kharkiv IS radar is located. The main technical information on the ionosonde are as follows: the range of sounding frequencies is 1.6–30 MHz and virtual altitude range is from 90 to 825 km with height resolution 1.4 km. In standard mode the ionosonde obtains one ionogram every 15 min.

3. Data and analysis method

In this study we consider the results of observations obtained by the Kharkiv IS radar, multipoint HF Doppler ionospheric sounding and ionosonde. The observations were carried out on September 18 and December 19, 2018. The main meteorological parameters that determine the tropospheric weather such as atmospheric pressure, temperature and wind speed over the observation region were considered. According to (https://meteopost.com/weather/archive/), there were no sharp changes in these parameters either in the days under observation or in the previous ones. The level of geomagnetic activity was evaluated using planetary A_p and K_p indices (Table 1) (https://wdc.kugi.kyoto-u.ac.jp). The extreme values of the geomagnetic activity indices were: $A_p = 5$, $K_p = 2+$, $D_{st} = -15$ and -12 nT for 18.09.2018 and 19.12.2018, respectively. The solar radio flux index $F_{10.7}$ was equal to 68.5 and 68.1. Solar wind speed reached a peak of 558.5 km/s at 01:20 UT and 523.8 km/s at 18:05 UT, total IMF reached 5.08 nT at 11:55 UT and 8.86 nT at 11:25 UT, the maximum southward component of B_z reached −3.98 nT at 05:55 UT and −4.25 nT at 07:00 UT for 18.09.2018 and 19.12.2018 respectively (https://omniweb.gsfc.nasa.gov/). Perturbations in the auroral electrojet were as follows: AE-index reached values of about 550 nT and 400 nT near 10 UT for September and December, respectively, which corresponds to slightly enhanced solar wind speed and negative B_z.

3.1. Radar measurements of ionospheric parameters

The IS radar measures spatiotemporal distributions of the following ionospheric parameters: the electron T_e and ion T_i temperatures, the electron concentration N_e, the vertical component of plasma transport velocity V_z and the ion percentage. The current study focuses on the temporal dependences of IS signal power. With the radar operating mode described above, it is possible to analyze variations within the altitude range from 100 to 400 km. At the first step, filtering was performed to restore the time-altitude dependencies. Used technique for determining TID propagation parameters is described in detail by Panasenko et al. (2018).

To identify wave processes the quasi-periodic variations in the relative power (δP) of the IS signal were analyzed. We studied wave processes in the range of periods of 10–120 min. The lower limit corresponds approximately to the Brunt–Väisälä period. The trend was determined as the approximation of the IS signal power by a polynomial of the 3rd order least squares method at an interval of 180 min with a step of 1 min. Finally, time series of relative variations of δP, obtained after trend subtracting and normalizing, were passed through a digital bandpass filter in the range 5–125 min, with subsequent narrowing (Aksonova and Panasenko, 2019).

To determine the predominant periods of oscillations and their time localization, an implementation of the adaptive Fourier transform (Chernogor, 2008) was used. That is, we used Fourier analysis with a sliding window and a width adjusted so that it was equal to a fixed number of harmonic periods. Fig. 2 shows the dynamic spectra δS_p distribution of IS signal power over a range of 5–125 min at different altitudes. In addition to time-period depen-

Table 1
State of the space weather.

Date	$F_{10.7}$	A_p	K_p
18.09.2018	68.5	5	2+ 2 2 2 1− 1− 1− 1 1
19.12.2018	68.1	5	1− 1+ 1+ 2 1− 2− 1+ 2

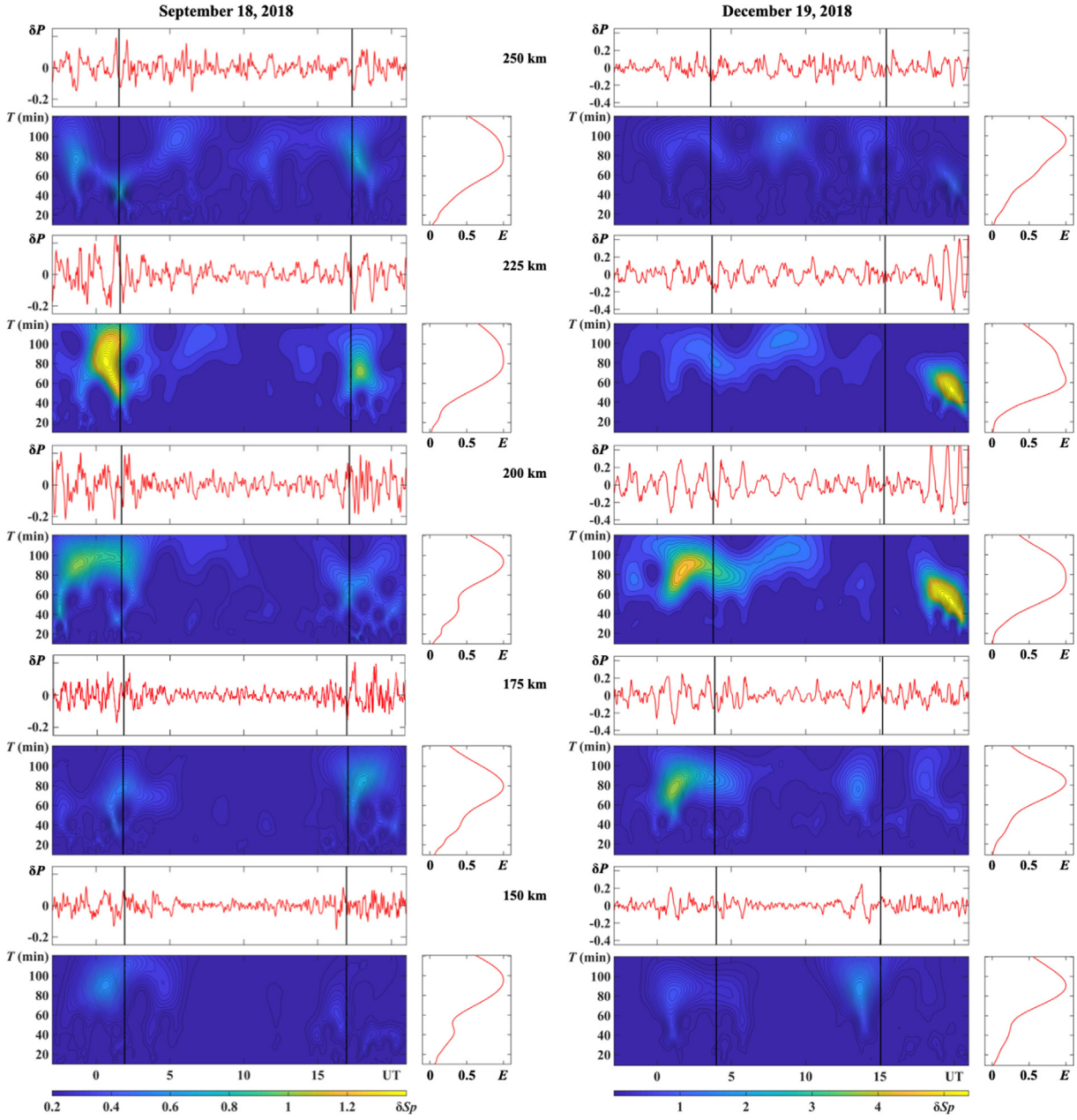

Fig. 2. The results of spectral analysis for altitudes of 150, 175, 200, 225 and 250 km for September 18 (left column) and December 19 (right column), 2018. For each height, the panel includes: relative variations of IS signal power δP; energy periodogram δS_P and energygram E of adaptive Fourier transform. Hereinafter, solid lines indicate the moments of passage of the local solar terminator at analyzed heights.

dences, we also analyzed energygrams, i.e., the distribution of signal energy over periods (See Fig. 3).

As shown in Fig. 2, the strongest quasi-periodic variations were observed near the sunrise and sunset terminators. The predominant periods lay in the interval from 60 to 100 min, for both days. However, there is a strong process with predominant period of about 50 min around 20 UT on December 19, 2018. As can be seen from the variations of relative values of IS signal power δP it twice prevailed in intensity over other oscillations (at heights of 200 and 225 km). In general, fluctuations in δS_p show higher intensity during winter observation.

3.2. Doppler HF measurements

The observations of the Doppler frequency shift (DFS) of HF signals made at spatially separated receiving points, which contain information about dynamic processes in the region of reflection of the probing signal from the ionosphere, were used. This technique allows us to detect disturbances at ionospheric heights, determine their period, and estimate velocity and propagation direction (Chum and Podolská, 2018).

To estimate DFS we analyzed the dynamic spectra of the registered HF signal. Data processing algorithm is

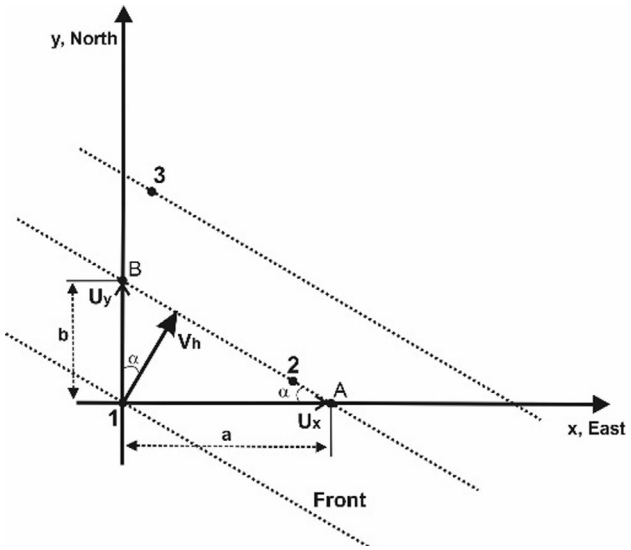

Fig. 3. Schematic geometry of plane wave propagation (amplitude front is shown by dashed line) with velocity V_h in the azimuthal direction α through three reflection points.

identical for all receiving sites and was as follows. The daily records of the HF signal were divided into fragments with duration of 30 s, for which the instantaneous power spectra were calculated. A rectangular window with a duration of 30 s and a 50 % overlap were used (i.e., the next spectrum is calculated for a time interval shifted by 15 s). The obtained Doppler spectrum sequences (spectrograms) within –5…+5 Hz bandwidth around the carrier frequency with a time resolution of 15 s and a frequency resolution of Δf≈0.033 Hz were used for automatic determination of the frequency of the main spectral maximum and its fluctuations in time. The algorithm of estimating of DFS of the signal reflected from the ionosphere is described by Chum and Podolská (2018) and Reznychenko et al. (2020) and consists mainly in the analysis of the three most intense spectral maxima in a given frequency range. The final choice of the maximum is made taking into account the frequencies and intensities of the neighboring spectra maxima. In the case of a multipath propagation such approach enables tracking of one spatial mode.

If the observed time series of DFS are characterized by quasiperiodic fluctuations, we assume a propagation of wave-like disturbances over the midpoint of corresponding radio path at ionospheric height. The period of disturbance is determined by the time interval between adjacent extrema of DFS variation or the moments of transition of the DFS through zero values. The simultaneous DFS values can be used to calculate radial velocity of the virtual reflecting point of the signal from the ionosphere.

The TIDs propagation parameters were estimated using time delays between similar quasiperiodic DFS variations registered at three spatially separated observation points (Sopin et al., 2012). A calculation of an azimuthal direction α and horizontal velocity V_h of wavelike ionospheric disturbances was made with the use of interferometric method in assumption that perturbation has a plane phase front and the three reflection points are located in midpoints of the corresponding radio lines (see Fig. 1, listed on the map by the numbers 1–3). The wave with plane front propagates with speed V_h in azimuthal direction α. The azimuthal direction is measured clockwise from north.

$$tg\alpha = \frac{u_y}{u_x};\ V_h = \frac{u_x u_y}{\sqrt{u_x^2 + u_y^2}},$$

where u_x, u_y - wavefront propagation velocity along x- and y- axis ($u_x = a/\tau_A$; $u_y = b/\tau_B$; τ_A, τ_B–time delay between DFS variations registered at points 1 and A, and 1 and B, respectively).

The equations for u_x and u_y in the case of an arbitrary location of the "receiving" sites can be obtained by using the intercept form of the equation of the line, which makes intercepts of a and b on the X and Y axis, respectively: x/a + y/b = 1. The positions of two wavefronts registered at point 2 and 3 with coordinates of observation point (reflection point) in Cartesian coordinate system associated with midpoint of KHR-LFO radio link (see Fig. 1, point 1) (x_2, y_2) and (x_3, y_3) can be written as $x_2/a2 + y_2/b2 = 1$ and $x_3/a3 + y_3/b3 = 1$. Substituting $a2 = u_x\tau_{21}$; $b2 = u_y\tau_{21}$; $a3 = u_x\tau_{31}$; $b3 = u_y\tau31$ (τ_{21}, τ_{31} - corresponding time delays between DFS variation) into above-mentioned expressions and derive system of equations the velocities u_x and u_y can be found as:

$$u_x = \frac{x_2y_3 - x_3y_2}{y_3\tau_{21} - y_2\tau_{31}};\ u_y = \frac{x_2y_3 - x_3y_2}{x_2\tau_{31} - x_3\tau_{21}}. \quad (1)$$

3.3. Ionosonde measurements

The Doppler ionosonde allows to save reflected signal amplitude, phase and Doppler shift as a two-dimensional array for further analysis. Since the output of the ionosonde stores information about the power of the reflected signal, we are able to obtain the dependences of altitude-time power variations in the sounding frequency band, the so-called height-time diagrams (Haldoupis et al., 2006). Also, to investigate TIDs in detail, we analyzed the temporal variations of the virtual height at different detection frequencies (isofrequency lines). Algorithm for constructing a virtual height-time chart of plasma frequencies of the extra-ordinary wave analyzed in this paper is described by Zalizovski et al. (2018).

4. Results

4.1. Altitude time parameters variations obtained by the IS method

Fig. 4 shows fluctuations of IS signal power δP within a period band of 5–125 min (a), 60–120 min (b) and 30–60 min (c) versus time and height. We can note from Fig. 4(a) that tilted phase front is clearly visible, even before narrower band filtration. As expected, phase fronts

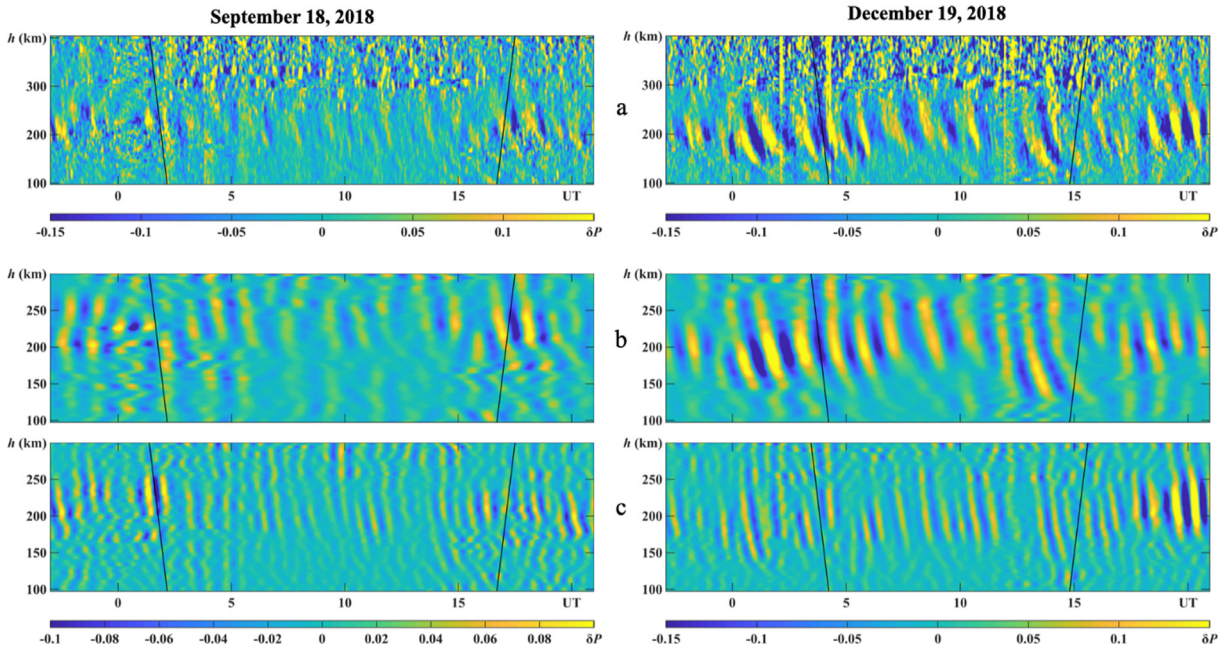

Fig. 4. Altitude-time dependence of 5–125 min (a), 60–120 min (b) and 30–60 min (c) bandpass filtered relative variations of IS power signal δ*P* for September 18 (left column) and December 19 (right column), 2018. Color scale shows intensity of amplitude variations (power).

have a downward vertical motion with respect to a fixed point of observation (Vadas and Nicolls, 2009; van de Kamp et al., 2014; Zhang et al., 2021). It is a typical feature of the TIDs generated by AGWs. The presence of wave activity in an altitude range of 150–300 km is traced. Above about 300 km altitude the TIDs in δ*P* variations are fading away, for both days. That's why Fig. 4(b) and (c) presents results of further band-pass filtered data for altitudes of 100–300 km. The following features were revealed. For September measurements TIDs for both period ranges were present near ST passage, while in the winter wave processes were present during the whole time of observations.

4.2. Height-time dependencies of plasma frequencies obtained by ionosonde

During the experiment of December 19, 2018 an operating regime of ionosonde has sampling rate 5 min that allows us studying the wave-like ionospheric disturbances with periods from 10 min. In the study the data of vertical sounding of the ionosphere in the form of height-time diagrams of ionospheric parameters were used. The virtual height-time diagram of frequencies of sounding signal reflected from the ionosphere (plasma frequencies) obtained from ionosonde data for December 19, 2018, is shown in Fig. 5. One can clearly see quasi-periodic fluctuations of virtual reflection heights for different frequencies between 18 and 22 UT indicating the presence of a wave-like processes in the ionosphere at virtual altitudes 230–320 km (it should be noted that the virtual height is greater than the real one, because the speed of light is used in the calculations). The temporal scale size of variations is approximately 50–60 min. As in the case of IS radar (see Fig. 4), the disturbance phase front estimated by virtual reflecting heights variations during 19–21 UT has a vertical component with downward direction of propagation, i.e. in case of TID associated with AGW the group velocity is directed upward (Negrea et al., 2016; Wei et al., 2021). The tilt of the phase front during two full oscillation periods remains stable. The obtained estimates of the vertical velocity based on the analysis of the time of observation of extrema of reflection height variations for different isofrequency levels is about 80–100 m/s.

4.3. Doppler spectrograms of HF signal

Fig. 6 shows spectrograms of HF signal (carrier frequency fc = 3777 kHz), registered in three sites: LFO (top panel), SWK (middle) and RAO (bottom panel) on December 19, 2018 during 19–23 UT.

Similar quasi-periodic DFS fluctuations detected at all receiving sites during the 20–22 UT, caused by propagation of wavelike disturbance overhead are clearly seen on spectrograms of HF signal. The period of variation is approximately 50 min and the magnitude is about 1 Hz. Note that before 19:50 UT on spectrograms there is no strong traces of ionospherically reflected signal. Probably during that time, the critical frequency was below the sounding frequency. Results of vertical ionospheric sounding support this assumption (see Fig. 5b).

The spectrum width of the recorded HF signal is quite wide and varies with time as well as its intensity. Nonetheless it is possible to determine DFS in all three receiving sites and estimate the time shifts between them.

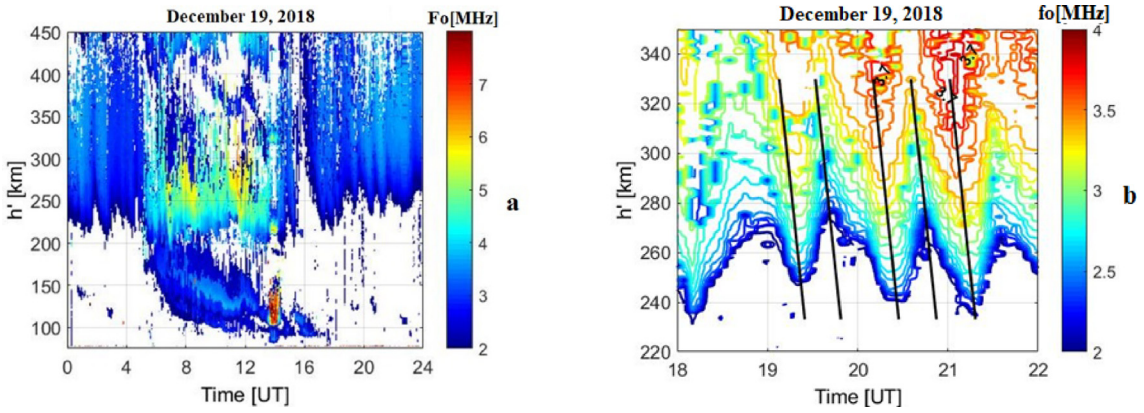

Fig. 5. (a) Virtual height-time diagram of plasma frequencies over Kharkiv region according to data of vertical ionospheric sounding on December 19, 2018; (b) temporal variations of virtual reflection height for different sounding isofrequency levels (from 2 to 4 MHz with step $\Delta f = 0.1$ MHz) from 18 to 22 UT. The black solid lines schematically indicate the tilt of the phase front. Color bars show the amplitude in MHz (frequency).

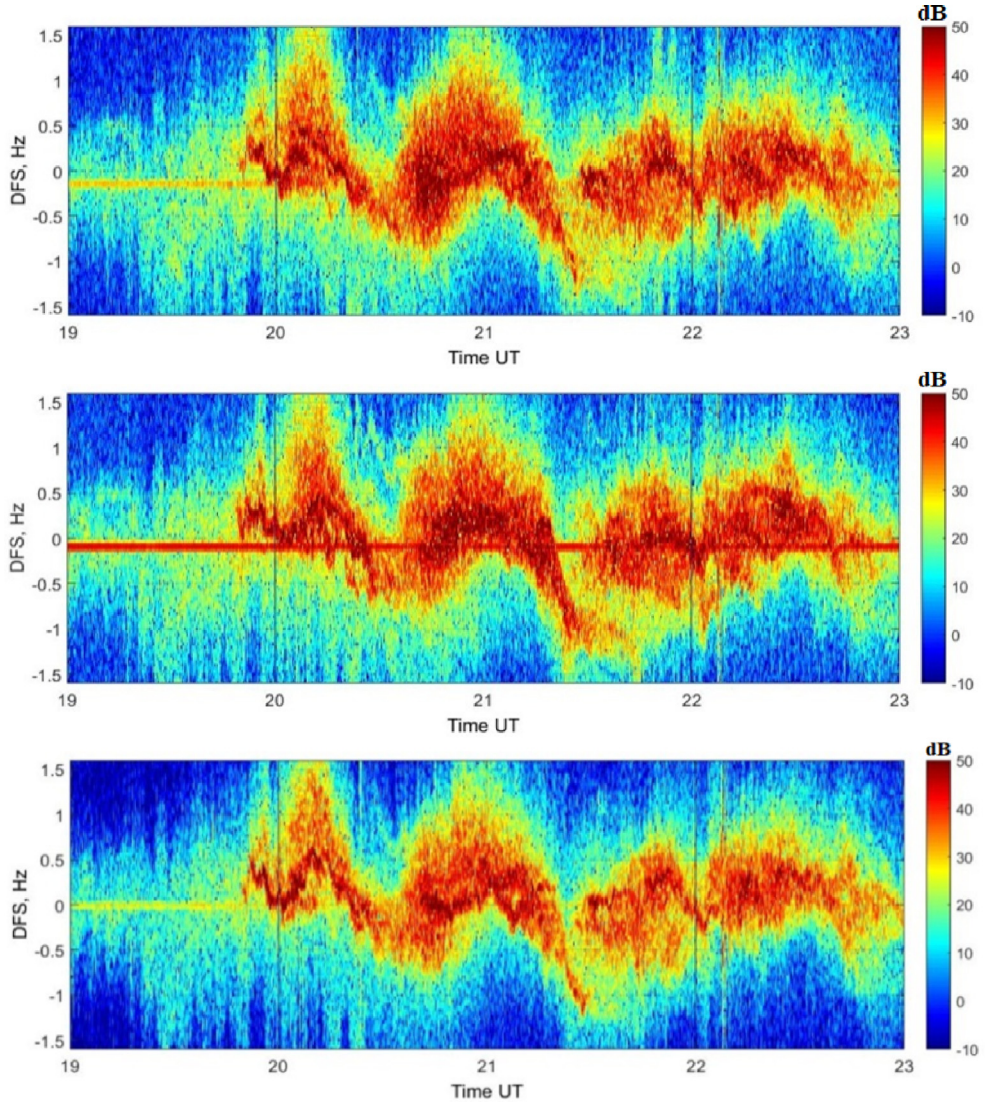

Fig. 6. Doppler spectrograms of HF signal (fc = 3777 kHz) recorded at LFO (top panel), SWK (middle) and RAO (bottom panel) on December 19, 2018, 19–23 UT. Color bars show the amplitude in dB (power).

It should be noted that since the variations of the DFS are almost synchronous, a standard time resolution of 15 s is not very suitable for determining the magnitude of the time shift between the DFS variations observed in three spatially separated points. Therefore, in order to increase the accuracy of determining the shift of the DFS series time resolution, the signal dynamic spectra were recalculated for the same width of the spectral window (30 s), but with a 29 -sec overlap of the intervals, i.e. with a step of 1 s. The time delays between DFS variations registered at the LFO-SWK and LFO-RAO stations (during 19.95–20.50 UT interval) estimated from the cross-correlation functions are approximately −61 and −8 s, respectively (DFS variations in the LFO are ahead).

The equations and estimates were obtained under the assumption of flat Earth. Assuming that reflection of the sounding signal occurs at the midpoint of the corresponding radio line (Fig. 1), estimations of horizontal velocity and azimuthal direction are ∼460 m/s and −102° correspondingly. The disturbance has a horizontal spatial scale size about 1380 km. Thus, the DFS variations observed in in evening 19.12.2018 is associated with a LSTID propagating in west-southwestward direction.

4.4. Characteristics of TIDs obtained with Kharkiv IS radar

Based on the most probable periods of TIDs obtained by spectral analysis (see Fig. 2), the appropriate subranges were chosen for further bandpass filtration in the range of 30–60 min and 60–120 min, which corresponds to large-scale structures. For determining the TID vertical propagation parameters we used cross-correlation analysis. We applied it to the bandpass filtered IS power relative variations (for both intervals) for evaluation of time lags at different heights relative to the height of 200 km. Horizontal phase velocities were estimated using a simple anelastic dispersion relation (Gossard and Hooke, 1975). This relation implies the knowledge about horizontal neutral wind velocity (U_h) vector and the angle between it and horizontal wave vector which were not measured in this study. We used data from the Horizontal Wind Model HWM14 (2014) for magnetically quiet conditions to partly overcome these issues. Since the angle is still unknown, we can estimate the horizontal wave phase velocity V_H with the absolute error that does not exceed U_h, i. e. $V_H = V_h \pm U_h$, where V_h is horizontal wave phase velocity estimation under zero wind condition. The same is true for horizontal wavelength Λ_H, which can be estimated with maximum absolute error $\Delta\Lambda_h = U_h T$. Thus, $\Lambda_H = \Lambda_h \pm \Delta\Lambda_h$, where $\Lambda_h = V_h T$.

We used several criteria in order to identify presence of TID event. Concerning ISR data, the value of relative amplitude $\delta P_{\max}$ of perturbation should exceed 0.05 (i.e., 5 %), at least two periods of duration and TIDs must cover a height range more than 40 km.

Table 2 indicates time intervals and height ranges of waves visibility, height h_{max} at which the relative amplitude of oscillations reaches the maximum values $\delta P_{\max}$, values of period T, vertical V_z and horizontal (for zero wind conditions) V_h phase velocities, horizontal wind velocity U_h, derived from HWM14 (2014) model, vertical Λ_z and horizontal (for zero wind conditions) Λ_h wavelengths, and maximum absolute errors in Λ_h estimations $\Delta\Lambda_h$. The symbols ↓ and ↑ denote TIDs, for which V_z was directed down and up, respectively.

The observed parameters place these TIDs both into the large and medium-scale class. The vertical component of the phase velocity V_z is directed downward for almost all observed perturbations, which corresponds to upward propagating AGWs. It should be noted that on time-altitude dependencies of IS power signal variations (see Fig. 4 for December), a wavelike ionospheric disturbance after 18 UT is much more clearly visible than on ionosonde data (see Fig. 5). The height range in which the disturbance is observed is 170–270 km, $h_{max} \sim 210$ km, predominant period is about 50 min and $V_z \sim 85$ m/s. Also, for one process (shown in Table 2 in bold) the upward direction of V_z propagation was found.

In general, the largest number of TIDs and the maximum values of their relative amplitudes were observed near the winter solstice. It is known that the meridional thermospheric wind in mid-latitudes in winter during daytime is much stronger, which contributes to wave propagation to higher altitudes due to altered wind filtration. Especially the maximum effect is achieved when the direction of the TID/AGW is opposite to the direction of the background neutral wind. The TID parameters mostly correspond to our previous results during magnetically quiet conditions (Aksonova and Panasenko, 2020). Despite this, there are some differences that will be considered in Discussion.

4.5. Comparison of TID characteristics

The results obtained by different techniques show common TID signature in the mid-latitude ionosphere during the solstice observation. Table 3 presents a comparison of TID parameters that were calculated by using all three methods. We found the presence of LSTID that propagate at approximately the same time, after evening ST passage 19 December 2018. For ISR and ionosonde measurements the signature was detected from 18 to 22 UT, while for multipoint Doppler sounding from 20 to 22 UT. As for the high-altitude propagation, the IS method is more accurate, since the ionosonde indicate a virtual height. Based on this, the TID spread at altitudes of 170–270 km. The dominant period was about 50 min according to all three methods.

Also, we found that estimated characteristics were similar. Vertical component of the phase velocity V_z was about 90 m/s and equal to 85 m/s, for ionosonde and ISR measurements, respectively. While the horizontal component of the phase velocity V_h was about 460 m/s for both IS and Doppler HF sounding system method. As for horizontal spatial scale it was equal $\Lambda_h = 1380$ km and $\Lambda_h = 1360$ km,

Table 2
TID parameters obtained by IS method.

Data	Time, UT	Height, km	T, min	h_{max}, km	δP_{max}	V_z, m/s	V_h, m/s	U_h, m/s	Λ_z, km	Λ_h, km	$\Delta\Lambda_h$, km	
18.09.18	**22:00–02:00**	**190–260**	**72**	**230**	**0.1**	**−55**	**420**	**96**	**230**	**1810**	**415**	↑
	03:00–07:00	200–270	76	257	0.08	45	350	101	210	1570	461	↓
	15:00–21:00	190–280	72	216	0.12	50	400	53	230	1750	229	↓
	00:00–05:00	165–250	52	230	0.14	85	460	58	260	1400	181	↓
	10:00–13:00	175–225	50	185	0.06	50	250	30	140	750	90	↓
	15:00–21:00	185–240	55	200	0.11	50	260	43	160	870	142	↓
19.12.18	23:00–07:00	150–260	80	185	0.27	35	320	26	170	1500	125	↓
	12:00–15:00	140–230	67	170	0.14	30	230	64	130	900	257	↓
	15:00–21:00	190–260	66	210	0.17	60	440	80	250	1720	317	↓
	00:00–05:00	140–235	50	195	0.12	50	280	21	150	840	63	↓
	07:00–16:00	150–240	45	175	0.1	50	250	83	140	680	224	↓
	18:00–22:00	170–270	50	210	0.37	85	460	49	260	1360	147	↓

based on the results obtained by Doppler HF and ISR measurements, respectively. Furthermore, we detected the typical downward propagating phase fronts of TIDs at virtual height-time diagram of plasma frequencies (see Fig. 5(b)), as well as at altitude-time dependence of relative variations of IS power signal (see Fig. 4).

5. Discussion

This work suggests that studying seasonal variability of the ionosphere state under low level of geomagnetic activity may reveal more about the coupling processes between the ionosphere and the lower atmosphere. Ionospheric perturbations can be caused by a combination of effects occurring in the auroral region, high-energy natural processes over the observation region and artificial effects caused by human activities. As it is known, the generation and propagation of gravity waves in the atmosphere depends on environmental parameters (Alexander et al., 2010). Atmospheric pressure pulsations, turbulence processes, surface atmosphere convection, local changes in atmospheric temperature etc., can be responsible for creating wave packets. Vadas and Liu (2009) investigated the mechanism of small- and medium-scale AGW generation associated with strong convective instability in the troposphere. The dissipation of such structures at altitudes of 120–250 km leads to the formation of secondary AGW. This AGW generation mechanism functions independently of geomagnetic conditions. They found the waves with a horizontal wavelength of ~2000 km and a period of ~80 min. AGW with such parameters lead to the formation of ionospheric disturbances belonging to the LSTIDs type.

Our results show differences in the periods, amplitudes and time of the occurrence of disturbances for both days of observations. The registered diurnal and seasonal patterns (larger amplitudes near the terminator and larger amplitudes in winter than in autumn) agree with patterns identified in previous statistical studies (Rishbeth and Mendillo, 2001; Medvedev et al., 2013; Ratovsky et al., 2015). As seen in Fig. 4 the relative amplitudes reach a minimum near noon and maximum at about 2 UT for morning hours for both days. While evening maximum is observed about 17 UT and 19 UT for autumn and winter, respectively. These results are in good agreement with finding of Afraimovich et al. (2009) that there is a rigid relationship between the generation of TIDs and solar terminator (ST) passage. An analysis of TIDs structure and the corresponding characteristics indicates that the ST is the probable source of the detected perturbations. In our case, the observation of the evening disturbance was 3 h after the passage of the evening ST at an altitude of 100 km for the solstice. But for the equinox, the waves appear before the ST. At the same time, it is worth noting similar parameters of TIDs from 15 to 21 UT for both seasons. In general, the time intervals, for both types of TIDs, as well as the periods found, were similar to results obtained in previous study (Aksonova and Panasenko, 2020). A significant difference was found only in the values of maximum amplitudes δP_{max} for LS oscillation before and after ST passage, which in this study are twice as large. Such results are very interesting, because in previous work (Aksonova and Panasenko, 2020) the observations were also carried out at a low level of solar activity (but $K_p = 3$). As for the autumn oscillation before the sunrise hours, similar ones were found by Panasenko et al. (2021). Also, TID patterns like "fishbone" structures were detected. They have been clearly seen during equinox near evening ST (Fig. 4). Vadas et al. (2018) has shown that such type of signatures is feature of the secondary gravity waves generation from local body forces and can be created in the stratosphere, mesosphere, and thermosphere.

Despite the fact that the experiments were performed at a low level of geomagnetic activity, the processes that constantly occur in the auroral zone can significantly affect the mid-latitude ionosphere, including the generation and propagation of AGWs/TIDs. Particularly under very low solar activity condition (Buresova et al., 2014) as it was in the case of the year 2018. According to [https://omniweb.gsfc.nasa.gov/form/omni_min_def.html], geomagnetic activity was at quiet to unsettled levels from 17 to 19

Table 3
Comparison of TID parameters registered near winter solstice by different methods.

Parameter	Method		
	ISR	Ionosonde	Doppler HF sounding system
Time, UT	18–22	18–22	20–22
Height, km	170–270	230–320	–
***T*, min**	50	50–60	50
V_z, m/s	85	90	–
V_h, m/s	460	–	460
Λ_h, km	1360	–	1380
Azimuth	–	–	−102°

September due to effects from a negative polarity coronal hole high speed stream (CH HSS). Solar wind speeds began the period on 17 September near 370 km/s, but, as previously noted in Section 3, increased to over 500 km/s following the onset of the CH HSS, reaching a peak speed of about 587 km/s. While during the solstice period 18–20 December, the speed of the solar wind grew from 400 to 600 km/s, with the highest value of 523.8 km/s at analyzed day. CH HSS can deposit more energy in Earth's magnetosphere over a longer interval. Therefore, it could be assumed that CH HSS contributed to the generation of more intense waves (larger values of estimated TID parameters, except for amplitudes) observed during daytime hours for the solstice (see Table 2). Also, variations in the *AE* index reached maximum values from 200 to 550 nT (with the peak about 10 UT) for equinox and reached a first peak of 470 nT (about 10 UT) and ranged from 100 to 270 nT (from 19 to 24 UT) for solstice. Dmitriev and Suvorova (2023) noted that even such moderate increase in the *AE* index (during quiet condition) leads to a change in total electron content (TEC) with an amplitude of >30 %.

In addition, this study provides convincing evidence that the methods of TIDs diagnostics discussed in this work, as well as processing methods for subsequent analysis of the obtained TID parameters, are correct. With simultaneous use of IS radar, ionosonde and multipoint Doppler sounding facilities a LSTID with the same periods during the same four-hour time interval was detected. A comparison of the TID characteristics obtained by the three methods shows a good correspondence. As can be seen from the Table 3, a difference between the ISR and ionosonde calculated vertical component of the phase velocity was only 5 m/s. While the horizontal wavelength calculated by the Doppler sounding system was 20 km higher than the value obtained by IS method.

6. Summary

This paper addresses the parameters of TIDs in the mid-latitude ionosphere over the Eastern Europe. The ionospheric data for autumnal equinox and winter solstice in 2018 were obtained using the Kharkiv incoherent scatter radar, multipoint facility for HF Doppler sounding and ionosonde. We found LSTIDs with dominant periods of 50–80 min and horizontal wavelength of 1360–1810 km, as well as MS TIDs with periods of 45–55 min and wavelength of 680 –900 km. The maximum values of relative amplitudes in received signal power of incoherent scatter radar vary from 6 to 14 % and from 10 to 37 % for September and December, respectively. More intense TID structures appeared near sunrise and sunset, the second one is stronger. The highlight of this study is that we were able to register LS oscillation (period of about 50 min) with identical parameters at different receiving point during solstice measurement. This disturbance propagated at altitudes of 170–270 km in the time interval of 18–22 UT (LT = UT + 2) with azimuthal direction −102°. The estimated vertical and horizontal components of the phase velocity and the horizontal spatial scale size were $V_z = 85$ m/s, $V_h = 460$ m/s and about $\Lambda_h = 1360$ km, respectively.

Utilization of three different methods, the results of which are very similar, supports reliability of presented results. The identification of the sources of such waves is of interest and needs further research. Further study of more cases of TIDs and comparison of the results with previous ones will make it possible to refine empirical models of the disturbances observed at mid-latitudes.

Declaration of competing interest

The authors declare that they have no known competing financial interests or personal relationships that could have appeared to influence the work reported in this paper.

Acknowledgements

The operation of Kharkiv ISR and Multipoint facility for HF Doppler sounding are supported by the Ministry of Education and Science and National Academy of Sciences of Ukraine. AOS and AVZ thank for the support of Grants 0121U108635, 0120U100231, 0122U001389, and 0122U002576 from the National Academy of Sciences of Ukraine, and Partner Projects P735 (EOARD 19IOE054) and P775 (EOARD 22IOE019) between EOARD, STCU and IRA NASU. Geomagnetic indices (A_p, K_p, *AE*, D_{st}) are downloaded from the World Data Center for Geomagnetism, Kyoto data archive (https://wdc.kugi.kyoto-u.ac.jp). The investigation was supported by the Horizon 2020 Framework Programme H2020-INFRAIA-2020-1 Project 101007599 – PITHIA-NRF TNA project LONG is acknowledged.

References

Afraimovich, E.L., Edemskiy, I.K., Leonovich, A.S., Leonovich, L.A., Voeykov, S.V., Yasyukevich, Y.V., 2009. MHD nature of night-time MSTIDs excited by the solar terminator. Geophys. Res. Lett. 36 (15). https://doi.org/10.1029/2009GL039803.

Aksonova, K.D., Panasenko, S.V., 2019. Manifestations of wave processes in ionospheric plasma parameters during the geospace storm on 1–3 September, 2016. Radio Phys. Radio Astron. 24 (1), 55–67. https://doi.org/10.15407/rpra24.01.055.

Aksonova, K.D., Panasenko, S.V., 2020. Predominant traveling ionospheric disturbances over Eastern Europe during low levels of solar and geomagnetic activities using incoherent scatter radar data. Radio Phys. Radio Astron. 25 (2), 100–117. https://doi.org/10.15407/rpra25.02.100.

Alexander, M.J., Geller, M., McLandress, C., Polavarapu, S., Preusse, P., Sassi, F., Sato, K., Eckermann, S., Ern, M., Watanabe, S., 2010. Recent developments in gravity-wave effects in climate models and the global distribution of gravity-wave momentum flux from observations and models. Quart. J. Roy. Meteor. Soc. 136 (650), 1103–1124. https://doi.org/10.1002/qj.637.

Azeem, I., Yue, J., Hoffmann, L., Miller, S.D., Straka III, W.C., Crowley, G., 2015. Multisensor profiling of a concentric gravity wave event propagating from the troposphere to the ionosphere. Geophys. Res. Lett. 42. https://doi.org/10.1002/2015GL065903.

Belehaki, A., Tsagouri, I., Altadill, D., Blanch, E., Borries, C., Buresova, D., et al., 2020. An overview of methodologies for real-time detection, characterisation and tracking of traveling ionospheric disturbances developed in the TechTIDE project. J. Space Weather Space Clim. 10, 42. https://doi.org/10.1051/swsc/2020043.

Bowman, G.G., 1990. A review of some recent work on mid-latitude spread-F occurrence as detected by ionosondes. J. Geomagn. Geoelec. 42 (2), 109–138. https://doi.org/10.5636/jgg.42.109.

Buresova, D., Lastovicka, J., Hejda, P., Bochnicek, J., 2014. Ionospheric disturbances under low solar activity conditions. Adv. Space Res. 54 (2), 185–196. https://doi.org/10.1016/j.asr.2014.04.007.

Chernogor, L.F., 2008. Advanced methods of spectral analysis of quasiperiodic wave-like processes in the ionosphere: Specific features and experimental results. Geomagn. Aeron. 48, 652–673. https://doi.org/10.1134/S0016793208050101.

Chum, J., Podolská, K., 2018. 3D Analysis of GW propagation in the ionosphere. Geophys. Res. Lett. 45 (21), 11562–11571. https://doi.org/10.1029/2018GL079695.

Dmitriev, A.V., Suvorova, A.V., 2023. Atmospheric effects of magnetosheath jets. Atmosphere 14, 45. https://doi.org/10.3390/atmos14010045.

Domnin, I., Chepurnyy, Y. M., Emelyanov, L. Y., Chernyaev, S., Kononenko, A., Kotov, D., et. al., 2014. Kharkiv incoherent scatter facility, Bulletin of the National Technical University "Kharkiv Polytechnic Institute". Series: Radiophysics and ionosphere, (downloadable from http://repository.kpi.kharkov.ua/handle/KhPI-Press/11199?locale=en/).

Fritts, D.C., Laughman, B., Wang, L., Lund, T.S., Collins, R.L., 2018. Gravity wave dynamics in a mesospheric inversion layer: 1. Reflection, trapping, and instability dynamics. J. Geophys. Res. Atmos. 123 (2), 626–648. https://doi.org/10.1002/2017JD027440.

Gossard, E.E., Hooke, W.H., 1975. Waves in the Atmosphere: Atmospheric Infrasound and Gravity Waves, Their Generation and Propagation. Elsevier Scientific Publ. Co., Amsterdam, Netherlands.

Haldoupis, C., Meek, C., Christakis, N., Pancheva, D., Bourdillon, A., 2006. Ionogram height–time–intensity observations of descending sporadic E layers at mid-latitude. J. Atmos. Sol. Terr. Phys. 68 (3–5), 539–557. https://doi.org/10.1016/j.jastp.2005.03.020.

Hines, C.O., 1960. Internal atmospheric gravity waves at ionospheric heights. Can. J. Phys. 38 (11), 1441–1481. https://doi.org/10.1139/p60-150.

Hocke, K., Schlegel, K., 1996. A review of atmospheric gravity waves and travelling ionospheric disturbances: 1982–1995. Ann. Geophys. 14 (9), 917–940. https://doi.org/10.1007/s00585-996-0917-6.

Hunsucker, R.D., 1982. Atmospheric gravity waves generated in the high-latitude ionosphere: a review. Rev. Geophys. 20 (2), 293–315. https://doi.org/10.1029/RG020i002p00293.

Koloskov, O., Kashcheyev, A., Bogomaz, O., Sopin, A., Gavrylyuk, B., Zalizovski, A., 2023. Performance analysis of a portable low-cost SDR-based ionosonde. Atmosphere 14 (1), 159. https://doi.org/10.3390/atmos14010159.

Koloskov, A.V., Yampolski, Y.M., Zalizovski, A.V., Galushko, V.G., Kascheev, A.S., La Hoz, C., et al., 2014. Network of internet-controlled HF receivers for ionospheric researches. Radio Phys. Radio Astron. 19 (4), 324–335. https://doi.org/10.15407/rpra19.04.324.

Lyons, L.R., Nishimura, Y., Zhang, S.R., Coster, A.J., Bhatt, A., Kendall, E., Deng, Y., 2019. Identification of auroral zone activity driving large-scale traveling ionospheric disturbances. J. Geophys. Res. Space Phys. 124, 700–714. https://doi.org/10.1029/2018JA025980.

Lyons, L.R., Nishimura, Y., Zhang, S.R., Coster, A., Liu, L., Bristow, W. A., Reimer, A.S., Varney, R.H., Hampton, D.L., 2021. Direct connection between auroral oval streamers/flow channels and equatorward traveling ionospheric disturbances. Front. Astron. Space Sci. 8, 738507. https://doi.org/10.3389/fspas.2021.738507.

Medvedev, A.V., Ratovsky, K.G., Tolstikov, M.V., Alsatkin, S.S., Scherbakov, A.A., 2013. Studying of the spatial-temporal structure of wavelike ionospheric disturbances on the base of Irkutsk incoherent scatter radar and digisonde data. J. Atmos. Solar-Terr. Phys. 105, 350–357. https://doi.org/10.1016/j.jastp.2013.09.001.

Medvedev, A.V., Ratovsky, K.G., Tolstikov, M.V., Oinats, A.V., Alsatkin, S.S., Zherebtsov, G.A., 2017. Relation of internal gravity wave anisotropy with neutral wind characteristics in the upper atmosphere. J. Geophys. Res. Space Phys. 122 (7), 7567–7580. https://doi.org/10.1002/2017JA024103.

Negrea, C., Zabotin, N., Bullett, T., Fuller-Rowell, T., Fang, T.W., Codrescu, M., 2016. Characteristics of acoustic gravity waves obtained from Dynasonde data. J. Geophys. Res. Space Phys. 121 (4), 3665–3680. https://doi.org/10.1002/2016JA022495.

Nenovski, P., Spassov, C.h., Pezzopane, M., Villante, U., Vellante, M., Serafimova, M., 2010. Ionospheric transients observed at mid-latitudes prior to earthquake activity in Central Italy. Nat. Hazards Earth Syst. Sci. 10, 1197–1208. https://doi.org/10.5194/nhess-10-1197-2010.

Nishimura, Y., Zhang, S.R., Lyons, L.R., Deng, Y., Coster, A.J., Moen, J.I., et al., 2020. Source region and propagation of dayside large-scale traveling ionospheric disturbances. Geophys. Res. Lett. 47, e2020GL089451. https://doi.org/10.1029/2020GL089451.

Ogawa, T., Nishitani, N., Otsuka, Y., Shiokawa, K., Tsugawa, T., Hosokawa, K., 2009. Medium-scale traveling ionospheric disturbances observed with the SuperDARN Hokkaido radar, all-sky imager, and GPS network and their relation to concurrent sporadic E irregularities. J. Geophys. Res. 114, A03316. https://doi.org/10.1029/2008JA013893.

Panasenko, S., Aksonova, K., Kotov, D., 2021. Characteristics of traveling ionospheric disturbances from incoherent scatter data: monograph, 148–148. (downloadable from https://publishing.logos-science.com/index.php/primedia/article/view/PaAkKo.monograph-2021).

Panasenko, S.V., Goncharenko, L.P., Erickson, P.J., Aksonova, K.D., Domnin, I.F., 2018. Traveling ionospheric disturbances observed by Kharkiv and Millstone Hill incoherent scatter radars near vernal equinox and summer solstice. J. Atmos. Sol. Terr. Phys. 172, 10–23. https://doi.org/10.1016/j.jastp.2018.03.001.

Ratovsky, K.G., Medvedev, A.V., Tolstikov, M.V., 2015. Diurnal, seasonal and solar activity pattern of ionospheric variability from Irkutsk Digisonde data. Adv. Space Res. 55 (8), 2041–2047. https://doi.org/10.1016/j.asr.2014.08.001.

Reznychenko, A.I., Koloskov, A.V., Sopin, A.O., Yampolski, Y.M., 2020. Statistic of seasonal and diurnal variations of Doppler frequency shift of HF signals at mid-latitude radio path. Radio Phys. Radio Astron. 25 (2), 118–135. https://doi.org/10.15407/rpra25.02.118.

Rishbeth, H., Mendillo, M., 2001. Patterns of F2-layer variability. J. Atmos. Solar-Terr. Phys. 63 (15), 1661–1680. https://doi.org/10.1016/S1364-6826(01)00036-0.

Shiokawa, K., Ihara, C., Otsuka, Y., Ogawa, T., 2003. Statistical study of nighttime medium-scale traveling ionospheric disturbances using midlatitude airglow images. J. Geophys. Res. 108 (A1), 1052. https://doi.org/10.1029/2002JA009491.

Somsikov, V.M., 2011. Solar terminator and dynamic phenomena in the atmosphere: a review. Geomagn. Aeron. 51, 707–719. https://doi.org/10.1134/S0016793211060168.

Sopin, A.O., Zanimonskiy, Y.M., Lisachenko, V.N., Yampolski, Y.M., 2012. Features of background variations in total electron content of ionosphere over the Antarctic Peninsula. Radio Phys. Radio Astron. 17 (1), 49–56. https://doi.org/10.15407/rpra.

Suzuki, S., Vadas, S.L., Shiokawa, K., Otsuka, Y., Kawamura, S., Murayama, Y., 2013. Typhoon-induced concentric airglow structures in the mesopause region. Geophys. Res. Lett. 40 (22), 5983–5987. https://doi.org/10.1002/2013GL058087.

Tsagouri, I., Belehaki, A., Koutroumbas, K., Tziotziou, K., Herekakis, T., 2023. Identification of Large-Scale Travelling Ionospheric Disturbances (LSTIDs) based on digisonde observations. Atmosphere 14 (2), 331. https://doi.org/10.3390/atmos14020331.

Vadas, S.L., Liu, H., 2009. Generation of largescale gravity waves and neutral winds in the thermosphere from the dissipation of convectively generated gravity waves. J. Geophys. Res 114, A10310. https://doi.org/10.1029/2009JA014108.

Vadas, S.L., Nicolls, M.J., 2009. Temporal evolution of neutral, thermospheric winds and plasma response using PFISR measurements of gravity waves. J. Atmos. Sol. Terr. Phys. 71 (6), 744–770. https://doi.org/10.1016/j.jastp.2009.01.011.

Vadas, S.L., Makela, J.J., Nicolls, M.J., Milliff, R.F., 2015. Excitation of gravity waves by ocean surface wave packets: Upward propagation and reconstruction of the thermospheric gravity wave field. J. Geophys. Res. Space Phys. 120, 9748–9780. https://doi.org/10.1002/2015JA021430.

Vadas, S.L., Zhao, J., Chu, X., Becker, E., 2018. The excitation of secondary gravity waves from local body forces: theory and observation. J. Geophys. Res.: Atmos. 123 (17), 9296–9325. https://doi.org/10.1029/2017JD027970.

van de Kamp, M., Pokhotelov, D., Kauristie, K., 2014. TID characterised using joint effort of incoherent scatter radar and GPS. Ann. Geophys. 32 (12), 1511–1532. https://doi.org/10.5194/angeo-32-1511-2014.

Waldock, J.A., Jones, T.B., 1986. HF Doppler observations of medium-scale travelling ionospheric disturbances at mid-latitudes. J. Atmos. Sol. Terr. Phys. 48, 245–260. https://doi.org/10.1016/0021-9169(86)90099-1.

Wei, L., Jiang, C., Hu, Y., Aa, E., Huang, W., Liu, J., et al., 2021. Ionosonde observations of spread F and spread Es at Low and middle latitudes during the recovery phase of the 7–9 September 2017 geomagnetic storm. Remote Sens. (Basel) 13 (5), 1010. https://doi.org/10.3390/rs13051010.

Zalizovski, A.V., Kashcheiev, A.S., Kashcheiev, S.B., Koloskov, A.V., Lisachenko, V.N., Paznukhov, V.V., et al., 2018. A prototype of a portable coherent ionosonde. Space Sci. Technol. 24 (3), 10–22. https://doi.org/10.15407/knit2018.03.010.

Zalizovski, A.V., Yampolski, Y.M., Mishin, E., Kashcheyev, S.B., Sopin, A.O., Koloskov, A.V., et al., 2021. Multi-position facility for HF Doppler sounding of ionospheric inhomogeneities in Ukraine. Radio Sci. 56, e2021RS007303. https://doi.org/10.1029/2021RS007303.

Zawdie, K.A., Belehaki, A., Burleigh, M., et al., 2022. Impacts of acoustic and gravity waves on the ionosphere. Front. Astron. Space Sci. 337. https://doi.org/10.3389/fspas.2022.1064152.

Zhang, S.R., Erickson, P.J., Gasque, L.C., Aa, E., Rideout, W., Vierinen, J., et al., 2021. Electrified postsunrise ionospheric perturbations at Millstone Hill. Geophys. Res. Lett. 48 (18), e2021GL095151. https://doi.org/10.1029/2021GL095151.